Efficient Spin-to-Charge Conversion via Altermagnetic Spin Splitting Effect in Antiferromagnet RuO_2

H. Bai,[1] Y. C. Zhang,[1] Y. J. Zhou,[1] P. Chen,[2] C. H. Wan,[2] L. Han,[1] W. X. Zhu,[1] S. X. Liang,[1] Y. C. Su,[1] X. F. Han,[2] F. Pan,[1] and C. Song[1,*]

[1]*Key Laboratory of Advanced Materials, School of Materials Science and Engineering, Tsinghua University, Beijing 100084, China*

[2]*Beijing National fLaboratory for Condensed Matter Physics, Institute of Physics, University of Chinese Academy of Sciences, Chinese Academy of Sciences, Beijing 100190, China*

(Received 22 December 2022; accepted 20 April 2023; published 22 May 2023)

The relativistic spin Hall effect and inverse spin Hall effect enable the efficient generation and detection of spin current. Recently, a nonrelativistic altermagnetic spin splitting effect (ASSE) has been theoretically and experimentally reported to generate time-reversal-odd spin current with controllable spin polarization in antiferromagnet RuO_2. The inverse effect, electrical detection of spin current via ASSE, still remains elusive. Here we show the spin-to-charge conversion stemming from ASSE in RuO_2 by the spin Seebeck effect measurements. Unconventionally, the spin Seebeck voltage can be detected even when the injected spin current is polarized along the directions of either the voltage channel or the thermal gradient, indicating the successful conversion of x- and z-spin polarizations into the charge current. The crystal axes-dependent conversion efficiency further demonstrates that the nontrivial spin-to-charge conversion in RuO_2 is ascribed to ASSE, which is distinct from the magnetic or antiferromagnetic inverse spin Hall effects. Our finding not only advances the emerging research landscape of altermagnetism, but also provides a promising pathway for the spin detection.

DOI: 10.1103/PhysRevLett.130.216701

Charge-spin interconversion plays a fundamental role in spintronic devices due to its importance in spin generation and detection [1,2]. Traditionally, the interconversion is realized via the spin Hall effect (SHE), the Rashba-Edelstein effect, as well as their inverse effects in heavy metals or interfaces [3–10]. These relativistic phenomena with time-reversal even ($\mathcal{T}$-even) have an obvious restriction: the generated or detected spin polarization is limited to the direction of $\widehat{J_C} \times \widehat{J_S}$ (σ_y), where $\widehat{J_C}$ and $\widehat{J_S}$ refer to flowing directions of the charge and the spin current, respectively [8,10]. To overcome it, one possible solution is utilizing the magnetic ordering to break the $\mathcal{T}$ symmetry. For instance, unusual charge-spin conversions based on magnetic or antiferromagnetic SHEs (M/AFM-SHE) have been reported in ferromagnetic (FM) trilayers and several antiferromagnets [11–18]. In these materials, spin current polarized to the directions of either $\widehat{J_C}$ (σ_x) or $\widehat{J_S}$ (σ_z) can be interconverted with the charge current. Nevertheless, M/AFM-SHE is also related to the relativistic spin-orbit coupling (SOC) in analogy to the traditional SHE, the magnitude of which is much weaker than that of the exchange coupling. Accordingly, it is desirable to realize the multifunctional charge-spin interconversion of σ_x and σ_z through the nonrelativistic magnetic spin splitting.

Recently, a novel collinear compensated magnetic phase with combined symmetry of both crystal and spin rotation as well as the broken spatial inversion-time reversal ($\mathcal{PT}$) symmetry, termed as altermagnet, has been extensively studied [19–21]. Owing to the alternating crystal potential from nonmagnetic atoms, several altermagnets like RuO_2 possess remarkable nonrelativistic spin splitting [22] with the magnitude of eV scale (comparable to FMs), giving rise to extraordinary magnetotransport behaviors [22–32]. Particularly, the nonrelativistic altermagnetic spin splitting effect (ASSE) enables the generation of spin current with characteristics of $\mathcal{T}$-odd and controllable polarization direction (parallel to the Néel vector) [23–27], the resultant spin splitting torque provides an efficient pathway for the field-free switching of perpendicular magnetization [26]. Conversely, spin-to-charge conversion induced by ASSE offers an efficient way to detect σ_x and σ_z, which can broaden functionalities of spintronic devices. Nevertheless, the experimental investigation is still lacking.

In this Letter, we experimentally report the spin detection process via ASSE in antiferromagnet RuO_2. By injecting pure spin current through the spin Seebeck effect (SSE), we show that the nontrivial spin-to-charge conversion of σ_x and σ_z is allowed in the $RuO_2(101)$/permalloy (Py) and $RuO_2(101)$/[Co/Pt] heterostructures, respectively. The conversion efficiency is anisotropic and relies on the crystal axes of RuO_2, which is well consistent with the symmetry of ASSE. Furthermore, the detected spin Seebeck voltage enhances with the decreasing of the temperature, indicating

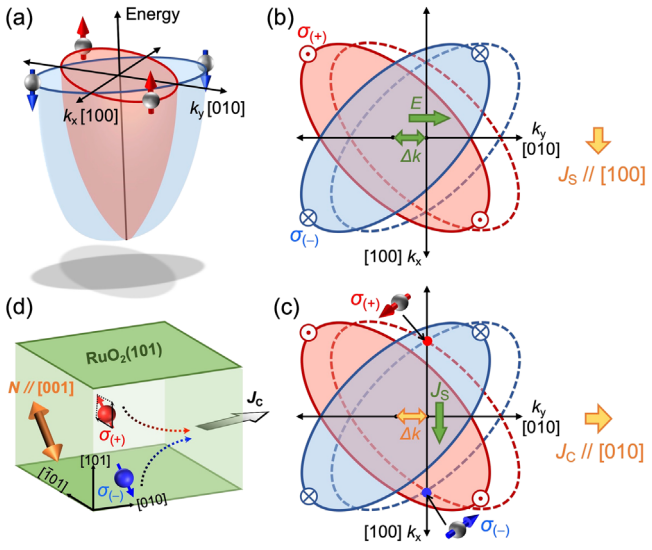

FIG. 1. Charge-spin interconversion via ASSE in RuO_2. (a) Anisotropic spin band splitting of RuO_2 at equilibrium. (b) Schematic diagrams of charge-to-spin conversion and (c) spin-to-charge conversion via ASSE in RuO_2 from the view of momentum space. (d) Schematic diagram of the spin-to-charge conversion via ASSE in the (101)-oriented RuO_2 film.

the conversion exhibits the features of nonrelativistic and $\mathcal{T}$-odd.

Ruthenium dioxide (RuO_2) is a typical rutile antiferromagnet with Néel temperature above 300 K [33,34]. The magnetic atom (Ru) is at the center of a stretched octahedron composed by the nonmagnetic atom (O). Notably, octahedrons of opposite sublattices are connected by rotation transformation, the resultant alternating crystal potentials cause the anisotropic magnetization densities and spin splitting Fermi contours at $k_z = 0$ [22,24], as shown in Fig. 1(a). This anisotropic spin band splitting is ascribed to ASSE, which brings about two reciprocal processes: (i) when we apply an electric field (E) along the [010] axis of RuO_2, the shift of Fermi contours (Δk) will produce a transverse spin current (J_S) polarized to the direction of the Néel vector [24–27], as illustrated in Fig. 1(b); (ii) when a pure spin current polarized parallel to the Néel vector is injected along the [100] axis of RuO_2, the spin accumulation or depletion will provoke the Fermi contours nonequilibrium and shifting, resulting in the generation of a charge current (J_C) along the [010] axis [Fig. 1(c)]. The detailed physical mechanisms of these two processes are depicted in Figs. S1–S3 of the Supplemental Material [35]. In this work, we mainly focus on the (101)-oriented RuO_2 film with the tilted Néel vector (N), which can realize the charge-to-spin conversion of both σ_x and σ_z [26,27]. Conversely, the $RuO_2(101)$ film enables the detection of spin current polarized away from the y axis (e.g., σ_x and σ_z), as long as the spin polarization has a projection on N [Fig. 1(d)], which is forbidden in the $\mathcal{T}$-even inverse SHE and the inverse Rashba-Edelstein effect. Accordingly, the $RuO_2(101)$ film provides a unique opportunity to distinguish ASSE from those $\mathcal{T}$-even effects.

To elucidate the ASSE-induced spin detection, we deposited 12 nm-thick $RuO_2(101)$ films on $Al_2O_3(1\bar{1}02)$ substrates. Further, ferromagnetic $Ni_{80}Fe_{20}$ (Py) layer with the in-plane magnetic anisotropy or Co/Pt multilayers with the perpendicular magnetic anisotropy were *in situ* grown (see Figs. S4 and S5 for details [35]). The control sample of $RuO_2/Y_3Fe_5O_{12}$(YIG) was grown on the GGG substrate, as displayed in Fig. S11 [35]. Subsequently, utilizing the standard lithography and Ar ion milling, these samples were fabricated into SSE devices (see Fig. S6 for details [35]).

We first present the detection of spin current with x-axial spin polarization in the $RuO_2(101)$/Py sample, the measurement geometry is shown in Fig. 2(a). The direction of the voltage channel (V) is defined as the x axis. The out-of-plane thermal gradient is generated by applying electric current in a heating electrode (Fig. S7 [35]), which can drive a nonequilibrium spin density and inject a pure spin current to the RuO_2 layer [36–38,44]. The polarization direction of the spin current is parallel to the magnetization direction of Py, which can be controlled by the external magnetic field H_{ext}. In this case, H_{ext} is applied parallel to V, ensuring the injected spin current is polarized along the x axis (σ_x).

Notably, ASSE-induced charge-spin conversion is highly relevant to the crystal axes of RuO_2 [24–27]. To demonstrate it, we fabricated multi-directional SSE devices to measure spin Seebeck voltages along different crystal axes [Fig. S6(d)]. For a device with angle φ, the geometric relationships between the voltage channel V, the external field H_{ext}, the in-plane projection of Néel vector (N_{ip}) and the [010] axis of RuO_2 are depicted in Fig. 2(b). Here φ is defined as the relative angle between V (also H_{ext}) and the [010]-axis. Theoretically, directions of N_{ip} and the converted charge current (J_C) are along [$\bar{1}$01] and [010] axes, respectively [24–27]. For devices at φ, the projection of σ_x on N_{ip} satisfies the relation of $\sin\varphi$, while the projected V on J_C has the relation of $\cos\varphi$. Accordingly, the dependence of spin Seebeck voltage V on φ follows: $V = C\sin\varphi\cos\varphi$.

Then we turn towards the experimental results. We show in Fig. 2(c) a typical loop of voltage V measured as a function of H_{ext} along the x-axis in the device with $\varphi = 60°$. And the applied heating current I_{heat} is +16 mA. According to the symmetry on H_{ext}, the raw data (V_{raw}) can be decomposed into the odd (V_{odd}) and even (V_{even}) components, which are the difference and sum of voltages measured at positive and negative H_{ext}, respectively (see Fig. S8 for details [35]). The V_{odd} term exhibits as a hysteresis loop with the coercive field of ~70 Oe, which is the exact value of magnetic hysteresis loop for RuO_2/Py sample [Fig. S4(c)]. With the magnetization (M) reversal, the polarization direction of injected spin current (σ) is also flipped between the $+x$ and $-x$ axes. It indicates the voltage difference between the positive and negative saturation field can be ascribed to the spin-to-charge

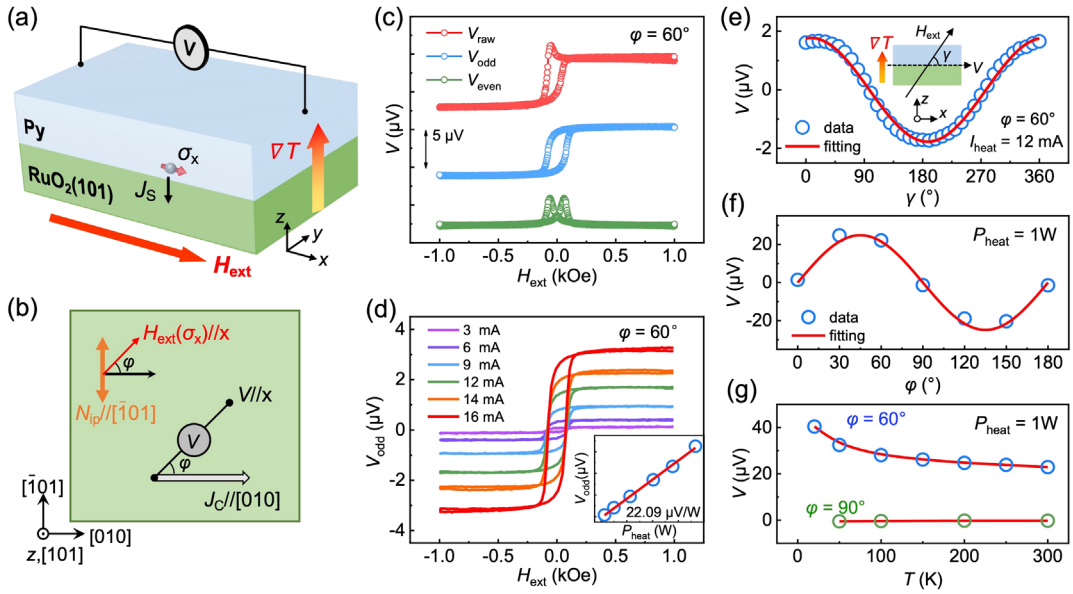

FIG. 2. Spin-to-charge conversion of σ_x. (a) Schematic diagram of SSE measurement configuration for the $RuO_2(101)$/Py sample. (b) Schematic diagram of SSE devices with different directional V. The direction of V is the x axis, and φ is the relative angle between V and the [010] crystal axis of RuO_2. (c) Thermal gradient-induced spin-dependent voltage for $I_{heat} = +16$ mA in the device with $\varphi = 60°$. (d) The dependence of V_{odd} on H_{ext} for various heating current (I_{heat}) measured in the device with $\varphi = 60°$. The inset summarizes values of V_{odd} at different heating power (P_{heat}). (e) The dependence of detected voltage V on the angle γ for $I_{heat} = 12$ mA in the device with $\varphi = 60°$. The inset shows the definition of the angle γ. (f) The dependence of V_{odd} on φ for $P_{heat} = 1$ W. The values are extracted from linear fitting of V_{odd} at each P_{heat} for devices with different φ. (g) Temperature-dependent V_{odd} for $P_{heat} = 1$ W in devices with $\varphi = 60°$ and $\varphi = 90°$.

conversion of positive or negative σ_x. Notably, this unusual conversion is absent in the SHE-based materials, such as heavy metals or even the rutile nonmagnetic IrO_2 [35,37,38,45]. Hence ASSE in antiferromagnetic RuO_2 is the most reasonable origin of the V_{odd} curve.

Accompanied with V_{odd}, an unexpected V_{even} term is also observed. By performing the SSE measurements with I_{heat} of -16 mA in the identical device, we show that V_{odd} remains unchanged while the sign of V_{even} is opposite, as plotted in Fig. S8 [35]. Since I_{heat} of ± 16 mA provokes the same thermal gradient, the I_{heat} polarity-independent result demonstrates that V_{odd} is purely from the thermal gradient-induced spin transport. In contrast, the I_{heat} polarity-dependent V_{even} term most likely arises from the anomalous Nernst effect (ANE) of the ferromagnetic Py layer (see Sec. S4 in the Supplemental Material for details [35]). Note that the ANE voltage signal from the antiferromagnetic RuO_2 layer can be excluded, because the orthogonal geometric relationship of ANE is unsatisfied and such a small external magnetic field (1 kOe) cannot manipulate the Néel vector of RuO_2 [Fig. S22].

To further support the above interpretation, we recorded voltage V with varying the relative angle γ between H_{ext} and V in the x–z plane, hence M (or the injected spin σ) has only x- and z-axial components, and ANE is forbidden symmetrically due to the lack of y-axial component of M. As shown in Fig. 2(e), the γ-dependent voltage curve can be well fitted by the relation of $C_1 \cos\gamma + C_2 \sin\gamma$, C_1 and C_2 represent the conversion efficiency of σ_x and σ_z, respectively [36,38]. The value of C_1 (1.76 μV) is comparable to the corresponding value of V_{odd} extracted from the V-H_{ext} curve (1.71 μV), indicating that the V_{odd} term stems from spin-to-charge conversion of σ_x.

We further measured the voltage at different heating power P_{heat} in the device with $\varphi = 60°$, the extracted V_{odd} terms are displayed in Fig. 2(d). It is clear that V_{odd} is linear to P_{heat}, and the slope can be used to semiquantitatively evaluate the spin-to-charge conversion efficiency, e.g., 22.09 μV/W or, equivalently, $V_{odd} =$ 22.09 μV when $P_{heat} = 1$ W. The identical measurements were carried out in devices with other φ, and the values of extracted V_{odd} are plotted in Fig. 2(f). Remarkably, these φ-dependent values can be well fitted by the relation of $V = C\sin\varphi\cos\varphi$, which is vital evidence for the observation of spin-to-charge conversion via ASSE in RuO_2 [25–27]. Furthermore, we measured the voltage as a function of temperature, as shown in Fig. 2(g). It is found that the spin Seebeck voltage significantly enhanced with the temperature decreasing for the device with $\varphi = 60°$, which is distinct to the heavy metal Pt or the rutile IrO_2 [46,47]. In these nonmagnetic materials, the spin-to-charge conversion induced by ISHE has the feature of temperature insensitivity. In contrast, the atypical temperature dependence in RuO_2 arises from the enhancement of the electron lifetime (or the reduction of the relaxation-time Γ) at lower temperature, which is quite the characteristic of

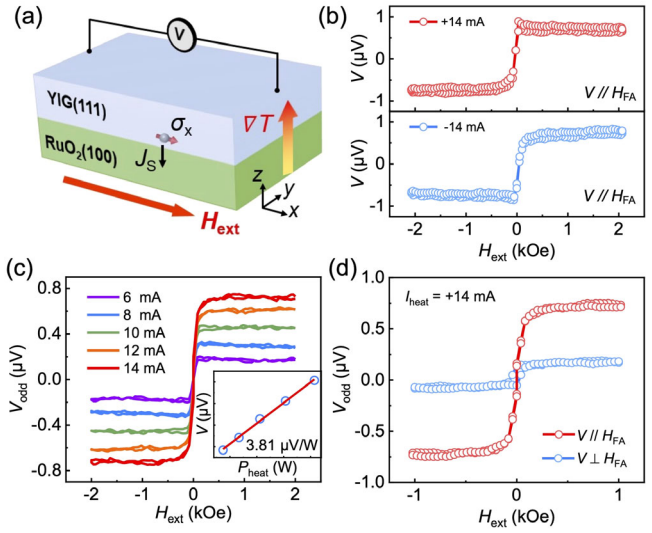

FIG. 3. SSE of the $RuO_2(100)/YIG(111)$ sample. (a) Schematic diagram of SSE measurement configuration for the $RuO_2(100)/YIG(111)$ sample. (b) Thermal gradient-induced spin-dependent voltage for $I_{heat} = \pm 16$ mA in the device with voltage channel V parallel to the direction of annealing field (H_{FA}). (c) The dependence of V_{odd} on H_{ext} for various I_{heat}. The inset summarizes values of V_{odd} at different heating power P_{heat}. (d) The dependence of V_{odd} on H_{ext} for devices with $V//H_{FA}$ and $V \perp H_{FA}$.

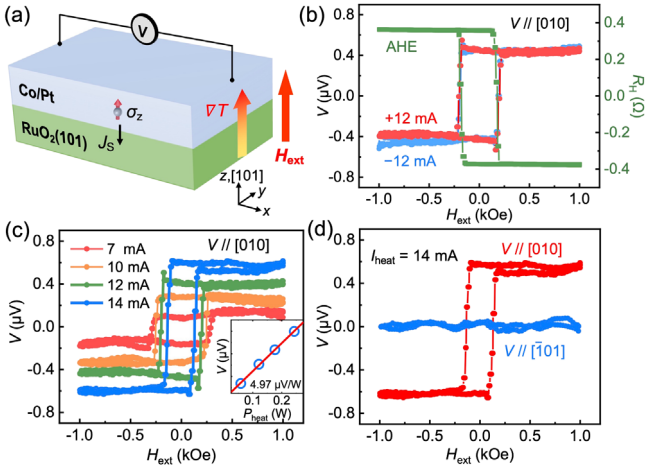

FIG. 4. Spin-to-charge conversion of σ_z. (a) Schematic diagram of SSE measurement configuration for the $RuO_2(101)/[Co/Pt]$ sample. (b) The dependence of the current-induced anomalous Hall resistance (R_H) and the thermal gradient-induced spin Seebeck voltage (V) on H_{ext} in the device with $V//[010]$. (c) The dependence of V on H_{ext} for various I_{heat} in the device with $V//[010]$. The inset summarizes values of V at different P_{heat}. (d) The dependence of V on H_{ext} in the device with $V//[010]$ and $V//[\bar{1}01]$.

the nonrelativistic ASSE with $\mathcal{T}$-odd [22,27]. As a control, spin Seebeck voltage measured in the device with $\varphi = 90°$ has negligible temperature dependence and all values are lower than 1 μV. In this case, ASSE-induced nontrivial spin-to-charge conversion is absent.

A control sample of RuO_2/YIG was used to exclude the ANE signals from the metallic Py layer. Here the RuO_2 layer grown on the YIG layer shows the (100)-oriented out-of-plane texture and polycrystalline in-plane orientation (Fig. S11 in [35]). After the magnetic field annealing (see Sec. S5 for details [35]), we performed SSE measurements with external magnetic field H_{ext} parallel to the voltage channel V, as depicted in Fig. 3(a). In the device of $V//H_{FA}$ ($\sigma_x//N$), sizable spin Seebeck voltages are observed [Fig. 3(b)]. Compared to that of the RuO_2/Py sample, the V_{even} term in this case is much decreased, because the ANE from the insulating YIG layer is negligible. Furthermore, the V_{odd} of the RuO_2/YIG sample is independent on the current-polarity [Fig. 3(b)] and linear to the heating power P_{heat} [Fig. 3(c)], supporting the origin from the spin-to-charge conversion of σ_x. In contrast, the V_{odd} is pretty small for the device of $V \perp H_{FA}$ ($\sigma_x \perp N$), as shown in Fig. 3(d). The difference exhibits the feature of ASSE, i.e., Néel vector-dependent spin-to-charge conversion.

To further clarify the spin-to-charge conversion via ASSE, we also performed SSE measurements with injected spins polarized to the z axis (σ_z) in the $RuO_2(101)/[Co/Pt]$ sample. As depicted in Fig. 4(a), the accumulation and injection of σ_z is induced by the out-of-plane thermal gradient. Here we focus on two measurement configurations: the voltage channel V is parallel or perpendicular to the [010] axis of RuO_2. Figure 4(b) shows the measured voltage V and the Hall resistance R_H as a function of H_{ext} in the case of $V//[010]$. When M is reversed by H_{ext}, a sizable jump of R_H appears at the coercive field of ~200 Oe. Meanwhile, the reversal of injected spin polarization induces opposite spin Seebeck voltage, giving rise to a hysteresis voltage loop with the same coercive field. The voltage curves are nearly identical for $I_{heat} = \pm 12$ mA, signifying the hysteresis loops purely arise from thermal gradient rather than the leakage current. This is supported by the measurements with varying the thermal gradient, where the spin Seebeck voltage V has the linear relation on P_{heat}, as shown in Fig. 4(c). For the geometry of $V//[\bar{1}01]$ (or $V \perp [010]$), the spin Seebeck voltage is negligible [Fig. 4(d)], due to the lacking of the converted charge current via ASSE in this axis (see Sec. S6 for details [35]).

To exclude the influence from the possible interfacial effect, control experiments were carried out in samples with Cu insertion, which can break the coupling between the antiferromagnet RuO_2 film and the ferromagnetic layers. As shown in Figs. S15 and S16 of the Supplemental Material, voltage loops arisen from the spin-to-charge conversion of both σ_x and σ_z remains. Besides, we show in Figs. S17 and S18 the RuO_2-thickness dependent measurements, which provides another evidence to exclude the possible interfacial effect. The crystal quality dependent measurements in Figs. S19–S21 demonstrate the magnitudes

of SSE voltages (proportional to the spin-to-charge conversion efficiency) are highly related to the crystal quality of RuO_2 films [35].

Apart from RuO_2, antiferromagnetic moment-related spin-to-charge conversion has been reported in noncollinear antiferromagnets [11,12] and collinear antiferromagnets with locally broken inversion symmetry [15], through the magnetic or antiferromagnetic inverse SHE (M/AFM-ISHE). We claim that ASSE is different to those effects based on the analysis below: (i) ASSE arises from the nonrelativistic magnetic spin splitting, while M/AFM-ISHE is relevant to the relativistic SOC. The magnitude of the former one is much larger than the latter one [19,20]. (ii) For ASSE, the detectable polarization direction of spin current (σ) is parallel to the Néel vector, while σ is perpendicular to the Néel vector or the cluster octupole moment for M/AFM-ISHE.

In conclusion, we present experimental results for the spin-to-charge conversion via ASSE in antiferromagnet RuO_2. Utilizing the spin Seebeck effect measurements, we demonstrate that the $RuO_2(101)$ film enables the nontrivial conversion of σ_x and σ_z into charge current, and the conversion efficiency is highly relevant to the crystal axes of RuO_2, which is well consistent with the symmetry of ASSE. Besides, the conversion efficiency enhances with the decreasing of temperature, signifying the features of nonrelativistic and $\mathcal{T}$-odd. The efficient charge-spin interconversion via ASSE not only enriches the emerging research landscape of altermagnetism, but also offers a powerful tool for the construction of multifunctional spintronic devices.

This work is supported by the National Key R&D Program of China (Grant No. 2022YFA1402603), the National Natural Science Foundation of China (Grant No. 52225106 and 12241404), and the Natural Science Foundation of Beijing, China (Grant No. JQ20010). C. S. acknowledges the support of Beijing Innovation Center for Future Chip (ICFC), Tsinghua University.

*songcheng@mail.tsinghua.edu.cn

[1] M. Johnson and R. H. Silsbee, Interfacial Charge-Spin Coupling: Injection and Detection of Spin Magnetization in Metals, Phys. Rev. Lett. **55**, 1790 (1985).

[2] F. J. Jedema, A. T. Filip, and B. J. van Wees, Electrical spin injection and accumulation at room temperature in an all-metal mesoscopic spin valve, Nature (London) **410**, 345 (2001).

[3] Y. K. Kato, R. C. Myers, A. C. Gossard, and D. D. Awschalom, Observation of the spin Hall effect in semiconductors, Science **306**, 1910 (2004).

[4] J. Wunderlich, B. Kaestner, J. Sinova, and T. Jungwirth, Experimental Observation of the Spin-Hall Effect in a Two-Dimensional Spin-Orbit Coupled Semiconductor System, Phys. Rev. Lett. **94**, 047204 (2005).

[5] S. O. Valenzuela and M. Tinkham, Direct electronic measurement of the spin Hall effect, Nature (London) **442**, 176 (2006).

[6] H. Zhao, E. J. Loren, H. M. Van Driel, and A. L. Smirl, Coherence Control of Hall Charge and Spin Currents, Phys. Rev. Lett. **96**, 246601 (2006).

[7] E. Saitoh, M. Ueda, H. Miyajima, and G. Tatara, Conversion of spin current into charge current at room temperature: Inverse spin-Hall effect, Appl. Phys. Lett. **88**, 182509 (2006).

[8] J. Sinova, S. O. Valenzuela, J. Wunderlich, C. H. Back, and T. Jungwirth, Spin Hall effects, Rev. Mod. Phys. **87**, 1213 (2015).

[9] J. C. R. Sánchez, L. Vila, G. Desfonds, S. Gambarelli, J. P. Attané, J. M. De Teresa, C. Magén, and A. Fert, Spin-to-charge conversion uing Rashba coupling at the interface between non-magnetic materials, Nat. Commun. **4**, 2944 (2013).

[10] A. Manchon, H. C. Koo, J. Nitta, S. M. Frolov, and R. A. Duine, New perspectives for Rashba spin-orbit coupling, Nat. Mater. **14**, 871 (2015).

[11] M. Kimata, H. Chen, K. Kondou, S. Sugimoto, P. K. Muduli, M. Ikhlas, Y. Omori, T. Tomita, A. H. MacDonald, S. Nakatsuji, and Y. Otani, Magnetic and magnetic inverse spin Hall effects in a non-collinear antiferromagnet, Nature (London) **565**, 627 (2019).

[12] J. Holanda, H. Saglam, V. Karakas, Z. Zang, Y. Li, R. Divan, Y. Liu, O. Ozatay, V. Novosad, J. E. Pearson, and A. Hoffmann, Magnetic Damping Modulation in $IrMn_3/Ni_{80}Fe_{20}$ via the Magnetic Spin Hall Effect, Phys. Rev. Lett. **124**, 087204 (2020).

[13] K. Kondou, H. Chen, T. Tomita, M. Ikhlas, T. Higo, A. H. MacDonald, S. Nakatsuji, and Y. C. Otani, Giant field-like torque by the out-of-plane magnetic spin Hall effect in a topological antiferromagnet, Nat. Commun. **12**, 6491 (2021).

[14] X. Chen, S. Shi, G. Shi, X. Fan, C. Song, X. Zhou, H. Bai, L. Liao, Y. Zhou, H. Zhang, A. Li, Y. Chen, X. Han, S. Jiang, Z. Zhu, H. Wu, X. Wang, D. Xue, H. Yang, and P. Feng, Observation of the Antiferromagnetic spin Hall effect, Nat. Mater. **20**, 800 (2021).

[15] L. Huang, Y. Zhou, H. Qiu, H. Bai, C. Chen, W. Yu, L. Liao, T. Guo, F. Pan, B. Jin, and C. Song, Antiferromagnetic inverse spin Hall effect, Adv. Mater. **34**, 2205988 (2022).

[16] A. M. Humphries, T. Wang, E. R. J. Edwards, S. R. Allen, J. M. Shaw, H. T. Nembach, J. Q. Xiao, T. J. Silva, and X. Fan, Observation of spin-orbit effects with spin rotation symmetry, Nat. Commun. **8**, 911 (2017).

[17] S. H. C. Baek, V. P. Amin, Y. W. Oh, G. Go, S. J. Lee, G. H. Lee, K. J. Kim, M. D. Stiles, B. G. Park, and K. J. Lee, Spin currents and spin-orbit torques in ferromagnetic trilayers, Nat. Mater. **17**, 509 (2018).

[18] H. Bai, Y. C. Zhang, L. Han, Y. J. Zhou, F. Pan, and C. Song, Antiferromagnetism: An efficient and controllable spin source, Appl. Phys. Rev. **9**, 041316 (2022).

[19] L. Šmejkal, J. Sinova, and T. Jungwirth, Beyond Conventional Ferromagnetism and Antiferromagnetism: A Phase with Nonrelativistic Spin and Crystal Rotation Symmetry, Phys. Rev. X **12**, 031042 (2022).

[20] L. Šmejkal, J. Sinova, and T. Jungwirth, Emerging Research Landscape of Altermagnetism, Phys. Rev. X **12**, 040501 (2022).
[21] L. Šmejkal, A. H. MacDonald, J. Sinova, S. Nakatsuji, and T. Jungwirth, Anomalous Hall antiferromagnets, Nat. Rev. Mater. **7**, 482 (2022).
[22] L. Šmejkal, R. González-Hernández, T. Jungwirth, and J. Sinova, Crystal time-reversal symmetry breaking and spontaneous Hall effect in collinear antiferromagnets, Sci. Adv. **6**, eaaz8809 (2020).
[23] M. Naka, S. Hayami, H. Kusunose, Y. Yanagi, Y. Motome, and H. Seo, Spin current generation in organic antiferromagnets, Nat. Commun. **10**, 4305 (2019).
[24] R. González-Hernández, L. Šmejkal, K. Výborný, Y. Yahagi, J. Sinova, T. Jungwirth, and J. Železný, Efficient Electrical Spin Splitter Based on Nonrelativistic Collinear Antiferromagnetism, Phys. Rev. Lett. **126**, 127701 (2021).
[25] H. Bai, L. Han, X. Y. Feng, Y. J. Zhou, R. X. Su, Q. Wang, L. Y. Liao, W. X. Zhu, X. Z. Chen, F. Pan, X. L. Fan, and C. Song, Observation of Spin Splitting Torque in a Collinear Antiferromagnet RuO_2, Phys. Rev. Lett. **128**, 197202 (2022).
[26] S. Karube, T. Tanaka, D. Sugawara, N. Kadoguchi, M. Kohda, and J. Nitta, Observation of Spin-Splitter Torque in Collinear Antiferromagnetic RuO_2, Phys. Rev. Lett. **129**, 137201 (2022).
[27] A. Bose, N. J. Schreiber, R. Jain, D. F. Shao, H. P. Nair, J. Sun, X. S. Zhang, D. A. Muller, E. Y. Tsymbal, D. G. Schlom, and D. C. Ralph, Tilted spin current generated by the collinear antiferromagnet ruthenium dioxide, Nat. Electron. **5**, 267 (2022).
[28] Z. Feng, X. Zhou, L. Šmejkal, L. Wu, Z. Zhu, H. Guo, R. González-Hernández, X. Wang, H. Yan, P. Qin, X. Zhang, H. Wu, H. Chen, Z. Meng, L. Liu, Z. Xia, J. Sinova, T. Jungwirth, and Z. Liu, An Anomalous Hall effect in altermagnetic ruthenium dioxide, Nat. Electron. **5**, 735 (2022).
[29] D. F. Shao, S. H. Zhang, M. Li, C. B. Eom, and E. Y. Tsymbal, Spin-neutral currents for spintronics, Nat. Commun. **12**, 7061 (2021).
[30] L. Šmejkal, A. B. Hellenes, R. González-Hernández, J. Sinova, and T. Jungwirth, Giant and Tunneling Magnetoresistance in Unconventional Collinear Antiferromagnets with Nonrelativistic Spin-Momentum Coupling, Phys. Rev. X **12**, 011028 (2022).
[31] I. I. Mazin, K. Koepernik, M. D. Johannes, R. González-Hernández, and L. Šmejkal, Prediction of unconventional magnetism in doped $FeSb_2$, Proc. Natl. Acad. Sci. U.S.A. **118**, e2108924118 (2021).
[32] R. D. Gonzalez Betancourt, J. Zubáč, R. Gonzalez-Hernandez, K. Geishendorf, Z. Šobáň, G. Springholz, K. Olejník, L. Šmejkal, J. Sinova, T. Jungwirth, S. T. B. Goennenwein, A. Thomas, H. Reichlová, J. Železný, and D. Kriegner, Spontaneous Anomalous Hall Effect Arising from an Unconventional Compensated Magnetic Phase in a Semiconductor, Phys. Rev. Lett. **130**, 036702 (2023).
[33] T. Berlijn, P. C. Snijders, O. Delaire, H. D. Zhou, T. A. Maier, H. B. Cao, S. X. Chi, M. Matsuda, Y. Wang, M. R. Koehler, P. R. C. Kent, and H. H. Weitering, Itinerant Antiferromagnetism in RuO_2, Phys. Rev. Lett. **118**, 077201 (2017).
[34] Z. H. Zhu, J. Strempfer, R. R. Rao, C. A. Occhialini, J. Pelliciari, Y. Choi, T. Kawaguchi, H. You, J. F. Mitchell, Y. Shao-Horn, and R. Comin, Anomalous Antiferromagnetism in Metallic RuO_2 Determined by Resonant X-Ray Scattering, Phys. Rev. Lett. **122**, 017202 (2019).
[35] See Supplemental Material at http://link.aps.org/supplemental/10.1103/PhysRevLett.130.216701 for detailed description of sample characterization, device fabrication, and spin Seebeck effect measurements, which includes Refs. [16,19,20,22,24–28,33,34,36–43].
[36] S. Y. Huang, W. G. Wang, S. F. Lee, J. Kwo, and C. L. Chien, Intrinsic Spin-Dependent Thermal Transport, Phys. Rev. Lett. **107**, 216604 (2011).
[37] D. Qu, S. Y. Huang, J. Hu, R. Wu, and C. L. Chien, Intrinsic Spin Seebeck Effect in Au/YIG, Phys. Rev. Lett. **110**, 067206 (2013).
[38] T. Kikkawa, K. Uchida, Y. Shiomi, Z. Qiu, D. Hou, D. Tian, H. Nakayama, X. F. Jin, and E. Saitoh, Longitudinal Spin Seebeck Effect Free from the Proximity Nernst Effect, Phys. Rev. Lett. **110**, 067207 (2013).
[39] T. C. Chuang, D. Qu, S. Y. Huang, and S. F. Lee, Magnetization-dependent spin Hall effect in a perpendicular magnetized film, Phys. Rev. Res. **2**, 032053(R) (2020).
[40] A. Yagmur, S. Sumi, H. Awano, and K. Tanabe, Magnetization-dependent inverse spin Hall effect in compensated ferrimagnet TbCo alloys, Phys. Rev. B **103**, 214408 (2021).
[41] A. D. Avery, M. R. Pufall, and B. L. Zink, Observation of the Planar Nernst Effect in Permalloy and Nickel Thin Films with In-Plane Thermal Gradients, Phys. Rev. Lett. **109**, 196602 (2012).
[42] H. Y. Ma, M. Hu, N. Li, J. Liu, W. Yao, J. F. Jia, and J. Liu, Multifunctional antiferromagnetic materials with giant piezomagnetism and noncollinear spin current, Nat. Commun. **12**, 2846 (2021).
[43] T. Kikkawa, K. Uchida, S. Daimon, Y. Shiomi, H. Adachi, Z. Qiu, D. Hou, X. F. Jin, S. Maekawa, and E. Saitoh, Separation of longitudinal spin Seebeck effect from anomalous Nernst effect: Determination of origin of transverse thermoelectric voltage in metal/insulator junctions, Phys. Rev. B **88**, 214403 (2013).
[44] K. Uchida, S. Takahashi, K. Harii, J. Ieda, W. Koshibae, K. Ando, S. Maekawa, and E. Saitoh, Observation of the spin Seebeck effect, Nature (London) **455**, 778 (2008).
[45] Z. Qiu, D. Hou, T. Kikkawa, K. I. Uchida, and E. Saitoh, All-oxide spin Seebeck effects, Appl. Phys. Express **8**, 083001 (2015).
[46] K. Uchida, H. Adachi, T. An, T. Ota, M. Toda, B. Hillebrands, S. Maekawa, and E. Saitoh, Long-range spin Seebeck effect and acoustic spin pumping, Nat. Mater. **10**, 737 (2011).
[47] P. Jiménez-Cavero, I. Lucas, J. Ara-Arteaga, M. R. Ibarra, P. A. Algarabel, and L. Morellón, Strong crystallographic influence on spin Hall mechanism in PLD-Grown IrO_2 thin films, Nanomater. Nanotechnol. **11**, 1478 (2021).